Optimum supply for an inverter-fed cage induction motor at different load conditions

M. Jahirul Islam and Antero Arkkio
Department of Electrical Engineering
Helsinki University of Technology
P. O. Box 3000, FIN-02015 TKK, Finland
Email: jahirul.islam@tkk.fi, antero.arkkio@tkk.fi

***Abstract*—The effects of power supply on the energy efficiency of a form-wound cage induction motor are studied when the motor operates under light loads. The cage induction motor is modelled with the space and time discretized finite-element analysis. The resistive losses are taken into account accurately by modelling eddy currents in the form-wound multi-conductor stator winding and the rotor cage. The core losses are considered with conventional empirical equations. A pulse-width-modulated (PWM) voltage is used to supply the motor. The fundamental harmonic (FH) terminal voltage is decreased from its rated value and the slip is adjusted to achieve a particular load condition. The variation of the total electromagnetic as well as the stator resistive losses are analyzed to find the optimum supply.**

***Index Terms*—optimum supply, finite-element analysis, PWM supply, electromagnetic losses, cage induction motor.**

I. Introduction

Usually, an induction motor is designed to maintain high efficiency when it runs in the region from 75 percent load to the full load [1-2]. However, the requirement of load may change with time. With changing load, the speed control is essential and control of the voltage is one possible technique [3]. When the requirement of the load is changed to a very light load condition, the efficiency of the induction motor becomes low. At no load or light load, a significant amount of losses can be saved by controlling the voltage [4-5]. The optimum supply of the machine will be different for different loadings of an electrical motor.

Due to the requirement of speed control, the application of inverter-fed electrical machines has increased significantly in recent years. When the motor is supplied from an inverter, the control of the motor becomes easy and accurate but the supply voltage is strongly non-sinusoidal and contains a set of harmonics [6-8]. These additional harmonics increase the electromagnetic losses of the motor significantly [9-13].

The pulse-width-modulation (PWM) is the most commonly used technique in an inverter. The most classic PWM modulation is based on comparing a sinusoidal modulating wave with high frequency triangular signal as a carrier. As a further improvement, one sixth of the third harmonic injection into the modulating wave has the advantages of achieving both greater fundamental and as well as reduced harmonics [13-15].

The main objective of this research is to study the variation of the electromagnetic losses to find the optimum supply for the different loads of an inverter-fed cage induction motor.

II. Methods

A. Modelling of cage induction motor

Time-discretized 2D finite-element analysis is used to model the cage induction motor where eddy currents in the stator winding are considered. The equation governing the electromagnetic field of a cage induction motor in a 2D model is

$$\nabla\times(\nu\nabla\times\vec{A})+\sigma\frac{\partial\vec{A}}{\partial t}-(\frac{1}{l_{\mathbf{e}}}\sum_{j=1}^{Q_{\mathrm{b}}^{\mathrm{r}}}\sigma\eta_j^{\mathrm{r}}u_j^{\mathrm{r}})\vec{e}_{\mathrm{z}}-(\frac{1}{l_{\mathbf{e}}}\sum_{j=1}^{Q_{\mathrm{b}}^{\mathrm{s}}}\sigma\eta_j^{\mathrm{s}}u_j^{\mathrm{b}})\vec{e}_{\mathrm{z}}=0 \tag{1}$$

where, $\vec{A}$ is the magnetic vector potential having only one nonzero component, ν is the reluctivity, t is time, l_{e} is the effective length of the machine, σ is the conductivity, $Q_{\mathrm{b}}^{\mathrm{r}}$ is the number of bars of the rotor winding in the solution region, $Q_{\mathrm{b}}^{\mathrm{s}}$ is the number of bars of the stator winding in the solution region, η_j^{r} and η_j^{s} are the functions to relate the nodal point of the rotor and stator bar *j*, u_m^{s} is the potential difference of the rotor bar *j*, u_j^{r} is the potential difference of the stator bar *j*.

The bar equation of the cage rotor is

$$u_j^{\mathrm{r}}=R_{\mathrm{b}}^{\mathrm{r}}i_{\mathrm{p}}^{\mathrm{r}}+R_{\mathrm{b}}^{\mathrm{r}}\int_{\vec{S}_p}\sigma\frac{\partial\vec{A}}{\partial t}\cdot\mathrm{d}\vec{S}_p\ ;p=1,...,Q_{\mathrm{b}}^{\mathrm{r}} \tag{2}$$

where, $R_{\mathrm{b}}^{\mathrm{s}}$ is the DC resistance of one rotor bar, $i_{\mathrm{p}}^{\mathrm{r}}$ is the current in the p^{th} rotor bar, $\vec{S}_p$ is the cross sectional area of the p^{th} rotor bar.

The equation of the stator phase is

$$u_m^{\mathrm{s}}=(Q_{\mathrm{s}}\sum_{j=1}^{Q_{\mathrm{b}}^{\mathrm{s}}}\sigma\eta_{jm}^{\mathrm{s}}u_j^{\mathrm{b}})+L_{\mathrm{e}}^{\mathrm{s}}\frac{\mathrm{d}i_{\mathrm{m}}^{\mathrm{s}}}{\mathrm{d}t}+R_{\mathrm{e}}^{\mathrm{s}}i_{\mathrm{m}}^{\mathrm{s}};m=1,...,Q_{\mathrm{m}} \tag{3}$$

where, Q_{s} is the number of symmetry sectors, Q_{m} is the number of phases, $i_{\mathrm{m}}^{\mathrm{s}}$ is the phase current of the m^{th} phase, $R_{\mathrm{e}}^{\mathrm{s}}$ is the DC resistance of one phase of the stator end winding, $L_{\mathrm{e}}^{\mathrm{s}}$ is the inductance of one phase of the stator end winding.

A separate voltage equation is considered for the stator bar,

which is strongly coupled with the field and the stator phase equations. The equation of the stator bar is

$$u_n^{\mathrm{b}} = (R_{\mathrm{b}}^{\mathrm{s}} \sum_{j=1}^{Q_{\mathrm{m}}} \eta_{nj}^{\mathrm{s}} i_j^{\mathrm{s}}) + R_{\mathrm{b}}^{\mathrm{s}} \int_{\vec{S_n}} \sigma \frac{\partial \vec{A}}{\partial t} \cdot \mathrm{d}\vec{S_n} \; ; m = 1, ..., Q_{\mathrm{b}}^{\mathrm{s}} \quad (4)$$

where, $R_{\mathrm{b}}^{\mathrm{r}}$ is the DC resistance of a stator bar of length l_{e}, η_{nj}^{s} is the function to relate between the stator bar *n* and phase *j* and $\vec{S_n}$ is the cross sectional area of the n^{th} bar of the stator winding. More detailed description can be found in [13], [16-18].

B. Stator resistive loss calculation

The resistive losses embedded in the stator slots are obtained by [16]

$$P_{\mathrm{sb}} = \frac{Q_{\mathrm{s}} l_{\mathrm{e}}}{\sigma} \sum_{j=1}^{Q_{\mathrm{b}}^{\mathrm{s}}} \int_{\Omega} \eta_i^{\mathrm{s}} \vec{J}^2 \mathrm{d}\Omega \quad (5)$$

where the current density in stator bar *i* is

$$\vec{J} = -\sigma \frac{\partial \vec{A}}{\partial t} + \sigma \frac{u_i^{\mathrm{s}} \vec{e}_{\mathrm{z}}}{l_{\mathrm{e}}} \quad (6)$$

The end winding resistive loss has been calculated from the DC resistance of the end winding and phase current

$$P_{\mathrm{ew}} = \sum_{i=1}^{m} R_e^{\mathrm{s}} (i_i^{\mathrm{s}})^2 \quad (7)$$

The total resistive loss of the stator winding is

$$P_{\mathrm{t}} = P_{\mathrm{sb}} + P_{\mathrm{ew}} \quad (8)$$

C. Rotor resistive loss calculation

The resistive losses of the rotor cage are

$$P_{\mathrm{rc}} = \int_V -\vec{J} \cdot \frac{\partial \vec{A}}{\partial t} \mathrm{d}V = \sum_{i=1}^{Q_{\mathrm{b}}^{\mathrm{r}}} \int_{V_i} \sigma \{ (\frac{\partial \vec{A}}{\partial t})^2 - \frac{u_i^{\mathrm{s}} \vec{e}_{\mathrm{z}}}{l_{\mathrm{e}}} \cdot \frac{\partial \vec{A}}{\partial t} \} \mathrm{d}V \quad (9)$$

where V_i is the volume of the i^{th} rotor bar inside the two-dimensional core region. Eq. (9) also includes the power fed to the ends of the rotor cage [8], [19].

D. Iron loss calculation

The iron core is modelled as non-conducting and non-linear materials having a single valued magnetization curve. Therefore, the iron losses are neglected in the solution of the magnetic field. An estimate for the iron losses is obtained from Fourier decomposition of the magnetic flux density in the iron core of the machine, using empirical models [8], [20] based on the Steinmetz formula

$$P_{\mathrm{FeH}} = \int_V \{ \sum_{i=1}^{N} C_{\mathrm{H}n} (n\omega_{\mathrm{s}}) \vec{B_n}^2 \} \mathrm{d}V \quad (10)$$

$$P_{\mathrm{FeE}} = \int_V \{ \sum_{i=1}^{N} C_{\mathrm{E}n} (n\omega_{\mathrm{s}}) \vec{B_n}^2 \} \mathrm{d}V \quad (11)$$

where P_{FeH} and P_{FeE} are respectively the hysteresis and eddy-current losses, $\vec{B_n}$ is the n^{th} harmonic of the magnetic flux density, *N* is the total number of Fourier components included in the analysis, $C_{\mathrm{H}n}$ is the hysteresis loss coefficient associated with the n^{th} harmonic, $C_{\mathrm{E}n}$ is the eddy-current loss coefficient associated with the n^{th} harmonic and ω_{s} is the fundamental angular frequency.

III. Results

A 3-phase, 50 Hz, 690 V, delta-connected 1250 kW cage induction motor is studied. The detailed dimensions of the machine and stator bars can be found in [13], [16-17].
The pulse-width-modulated voltage supply is obtained by making the comparison between the sinusoidal modulating signal and high-frequency triangular signal as a carrier (switching) frequency. To increase the value of the fundamental term and decrease the harmonic contents, 1/6 of the third harmonic is injected to the modulating signal [13-14], [21]. The switching frequency is 2 kHz for the studies. A schematic diagram of an inverter fed motor is presented in Fig. 1. The line-to-line voltage at the terminal is presented in Fig. 2 as a function of time when the motor is supplied from the PWM voltage source inverter at the rated voltage (690 V). The fast Fourier transformation (FFT) of the line-to-line voltage is presented in Fig. 3. The spectrum has been obtained from the complex valued of the space vector.

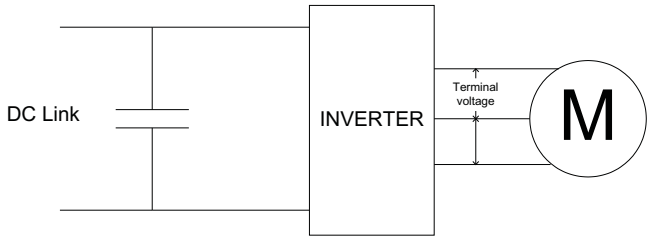

Fig. 1. Schematic diagram of an inverter fed motor.

To find the optimum supply, the FH terminal voltage is decreased from the rated voltage and the slip is increased to keep the shaft power constant. The value of the slip is fine-tuned to achieve the required load point.

A. Fixed DC-link voltage

Most of the drive systems have a particular and fixed DC-link voltage. To search for the optimal power supply of an inverter-fed cage rotor induction motor, the DC-link voltage is kept constant at 975 V. The flux-weakening frequency is chosen to increase from 50 Hz to decrease the fundamental harmonic (FH) terminal voltage. To keep the shaft power constant, the slip has been adjusted. Approximately, for a quarter load the shaft power was about 290 kW and for half

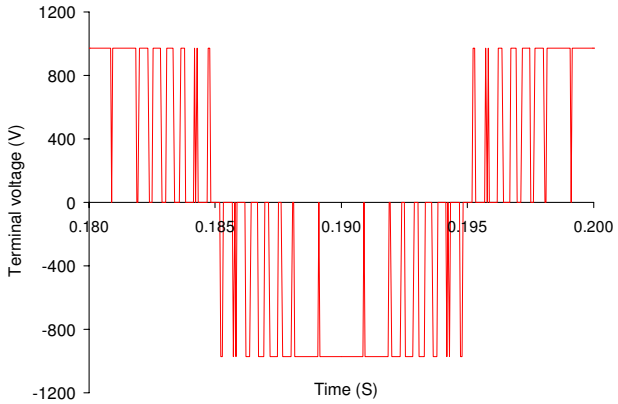

Fig. 2. The line voltage at the terminal of the machine is presented as a function of time when the motor is supplied from a PWM voltage source at the rated voltage (690 V).

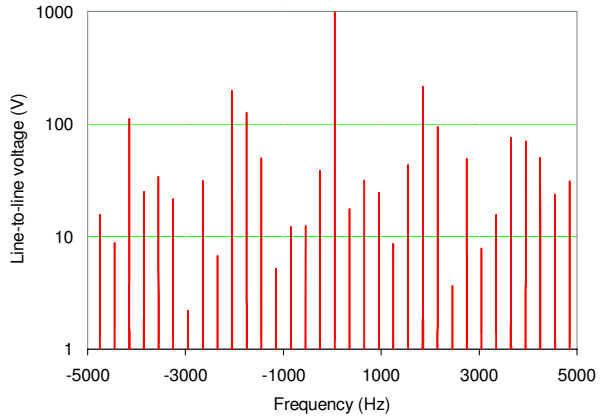

Fig. 3. The fast Fourier transformation (FFT) of the line-to-line voltage when the motor is supplied from a PWM voltage source at the rated voltage (690 V).

load it was about 590 kW.

The line-to-line voltage at the terminal of the motor is presented as a function of time in Fig 4a when the FH terminal voltage is 505 V and in Fig. 4b when it is 298.5 V. By comparing Fig. 2 and Fig. 4 it can be observed that the DC-link voltage is fixed but FH terminal voltage is changed by changing the modulation. The corresponding FFT spectrum of the line-to-line voltage at the terminal is presented in Fig. 5a when the FH terminal voltage is 505 V. For the FH line-to-line voltage 298.5 V, the FFT is presented in Fig. 5b. The FFT has been obtained from the complex valued space vector. It can be seen from the FFT spectrum (Fig. 3 and Fig. 5), that a decrease of the FH increases the higher harmonics. The variation of the stator resistive loss as a function of the FH terminal voltage is presented in Fig. 6. The variation of the total electromagnetic loss is presented in Fig. 7 as a function of the FH terminal voltage. The decomposition of the total electromagnetic loss into components is presented in Fig. 8.

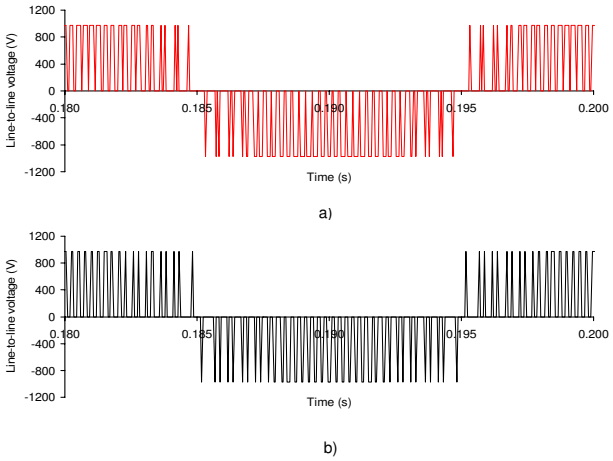

Fig. 4. The line-to-line voltage at the terminal of the motor presented as a function of time when the FH terminal voltage is a) 505 V and b) 298.5 V. A constant DC-link voltage (975 V) is maintained

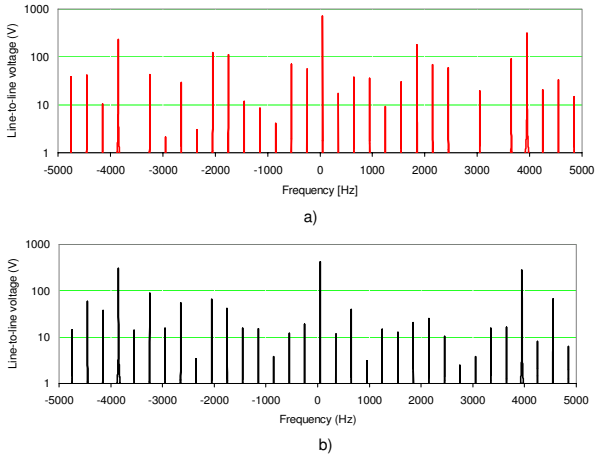

Fig. 5. The FFT of the line-to-line voltage at the terminal when the FH terminal voltage is a) 505 V and b) 298.5 V. A constant DC-link voltage (975 V) is maintained.

At the quarter load, the reduction of the stator resistive loss is possible but the amount is not very significant. Whereas, at half load it increases when the FH terminal voltage decreases. The core losses decrease with a decreasing FH terminal voltage. As a result, the total electromagnetic loss is reduced approximately 23 percent at quarter load, whereas it is reduced about 8 percent for the half load. The percent of loss reduction is calculated by comparing the loss at the rated voltage (690 V) for a particular load. The calculation of the core losses may have accuracy problems, as the harmonics of order greater than 90 are neglected. Due to the computational

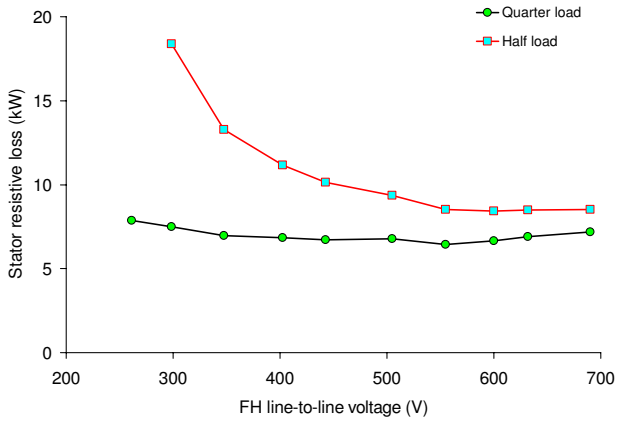

Fig. 6. The variation of the stator resistive losses as a function of the fundamental harmonic (FH) terminal voltage. The shaft power is maintained at quarter and half of the rated load. A constant DC-link voltage (975 V) is maintained.

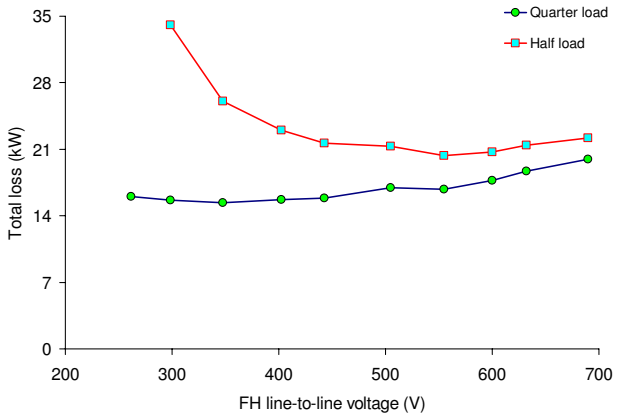

Fig. 7. The variation of the total electromagnetic losses as a function of the FH terminal voltage for the quarter and half load. A constant DC-link voltage (975 V) is maintained.

complexity, the harmonics are considered only below 4.5 kHz (90X50 Hz) for the calculation of core loss.

B. Changeable DC-link voltage

The FH terminal voltage is decreased from its rated voltage (690 V) by decreasing the DC-link voltage whereas the flux-weakening frequency is kept constant at 50 Hz. The value of the slip is adjusted to achieve the desirable shaft power. Approximately, for the quarter load the shaft power was about 295 kW, for half load about 595 kW and for three quarter load the shaft power is 890 kW. The line-to-line voltage at the terminal is presented as a function time in Fig. 9a when the FH terminal voltage is 510 V and in Fig. 9b when it is 320 V. The variation of the stator resistive losses as a function of the FH terminal voltage is presented in Fig. 10 for the quarter,

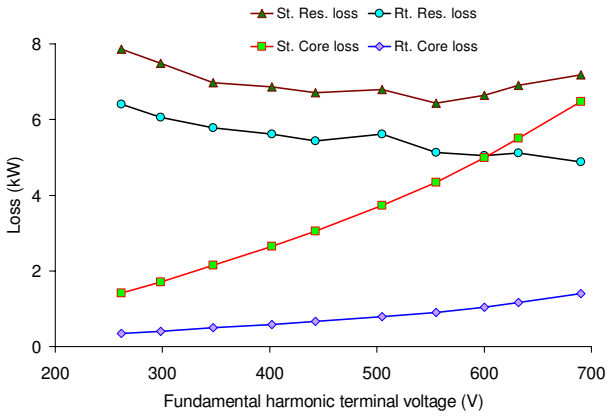

Fig. 8. Decomposition of the total electromagnetic losses into components for the quarter load as a function of FH terminal voltage. A constant DC-link voltage (975 V) is maintained.

half and three-quarter loads. For exactly the same load points the variation of the total electromagnetic loss is presented in Fig. 11 as a function of the FH terminal voltage.

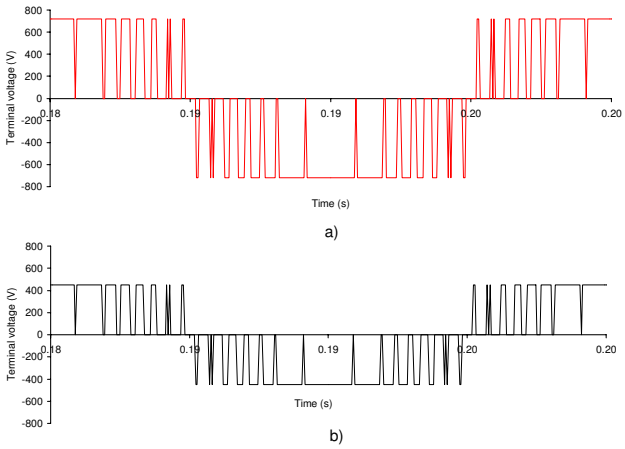

Fig. 9. The line voltage at the terminal of the machine is presented as a function of time when the FH terminal voltage is a) 510 V and b) 320 V.

The slip is adjusted to maintain the particular load points for different FH terminal voltages. The variation of slip, adjusted with the FH terminal voltage to maintain a particular shaft power, is presented in Fig. 12 as a function of the FH terminal voltage. The decomposition of the total electromagnetic loss into its components is presented in Fig. 13 as a function of the FH terminal voltage. The influence of the different components can be seen by comparing to Fig. 5. The resistive losses decrease significantly if it is possible to use a changeable DC-link voltage for the light load condition. The core losses are decreased almost in a similar way as for fixed DC-link voltage.

The reduction of the stator resistive losses in percent of the

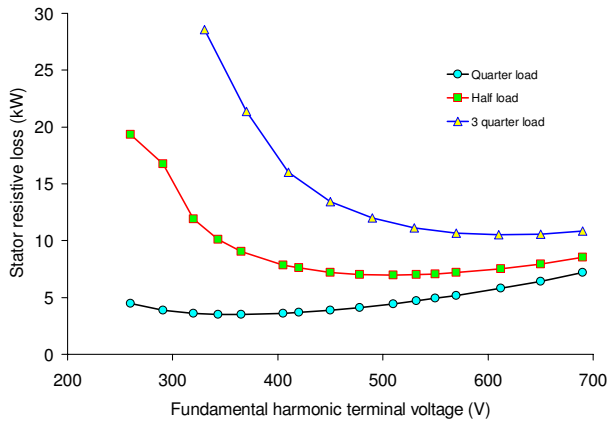

Fig. 10. The stator resistive losses presented as a function of FH terminal voltage. The shaft power is maintained at about quarter, half and three quarters of the rated load.

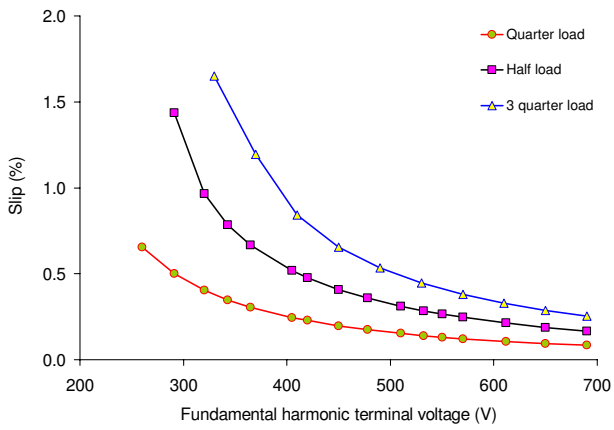

Fig. 12. Variation of slip as a function of FH terminal voltage for different load condition.

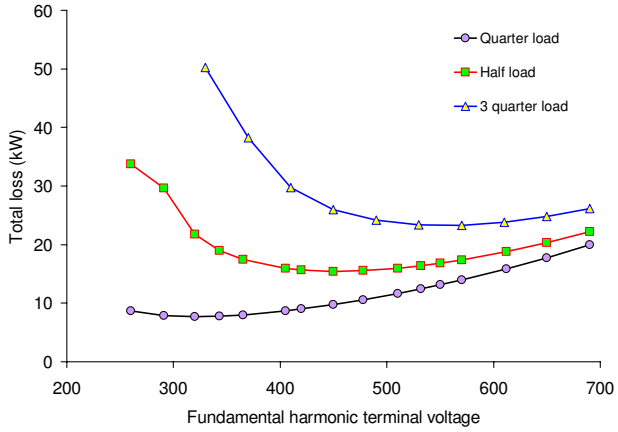

Fig. 11. The total electromagnetic losses presented as a function of FH terminal voltage. The shaft power is maintained at about quarter, half and three quarters of the rated load.

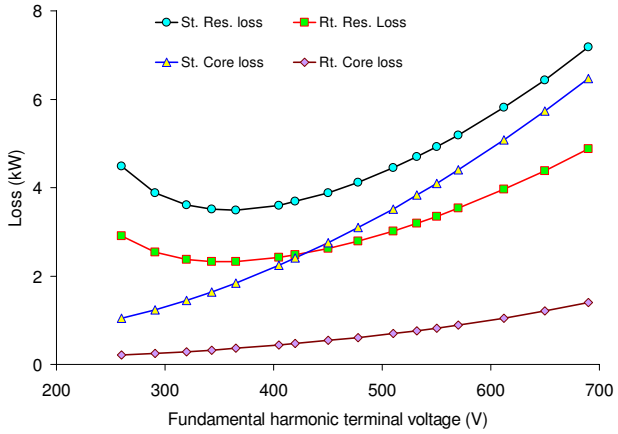

Fig. 13. The total electromagnetic loss, decomposed into components is presented as a function FH terminal voltage. The shaft power is at about quarter of the rated load.

stator resistive losses at the rated voltage (690 V) is presented in Fig. 14 as a function of the FH terminal voltage for the changeable DC-link voltage at quarter, half and three quarters of the rated load. In Fig. 15, the reduced total electromagnetic loss in percent of the total electromagnetic loss at the rated voltage (690 V) is presented for the quarter, half and three-quarter loads.

To study the influence of PWM supply compared to the sinusoidal supply, the stator resistive losses are presented in Fig. 16 as a function the FH terminal voltage at the quarter load.

IV. Discussion

The machine is studied at quarter and half of the rated load for the constant DC-link voltage. For the fixed DC-link voltage, the higher harmonics increase with the decrease of the FH terminal voltage. As a result, the resistive loss in the cage rotor is increased. Anyway, due to the contribution of the FH, the stator resistive loss can be reduced. However, the reduction of the stator resistive loss is not very significant. Since the core losses are decreased with a decrease of the FH terminal voltage, the total electromagnetic loss is decreased about 23 percent for the quarter load and approximately 8 percent for the half load.

If there is a possibility to change the-DC link voltage with the FH terminal voltage, the electromagnetic losses can be reduced significantly for the light load conditions. The stator resistive losses are reduced about 51 percent at the quarter load and about 18 percent at the half load. The stator resistive losses are compared with the losses at the rated voltage (690 V). The total electromagnetic losses are reduced to about 61 percent at the quarter load and about 31 percent at half of the rated load. When the load point is changed, the optimum

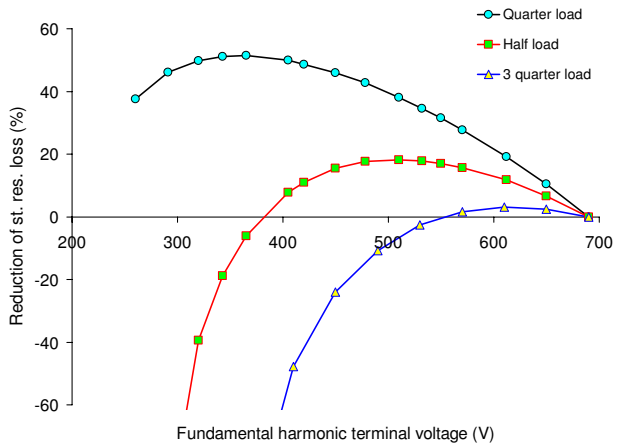

Fig. 14. The reduction of stator resistive losses in percent compared to the rated voltage (690 V) presented as a function of FH terminal voltage. The value of the slip has been increased when decreasing the voltage. The study has been done for the quarter, half and three-quarter load.

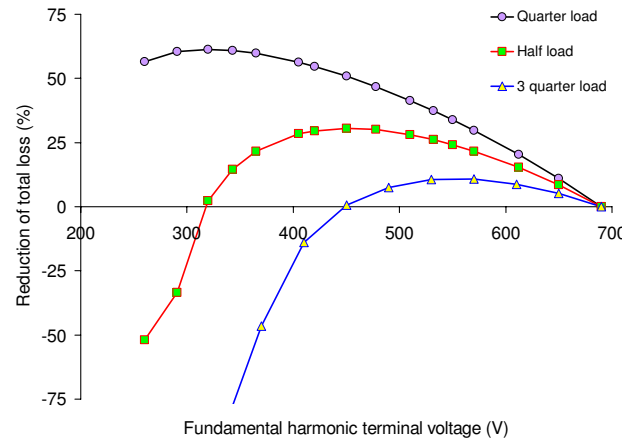

Fig. 15. The reduction of total electromagnetic losses in percent compared to the rated voltage (690 V) presented as a function of FH terminal voltage. The shaft power is at about quarter, half and three quarters of the rated load.

supply also changed. However, if the load point is greater than 75 percent of the rated load, there is very little scope to improve. If the motor is running at a very light load conditions, the electromagnetic losses can be reduced significantly by controlling the speed and voltage if there is a possibility to use the changeable DC-link voltage in the inverter.

V. Conclusion

The results presented are obtained by making the simulation with the space and time-discretized finite-element analysis. A 1250 kW form-wound cage induction motor is used for the study. The eddy-currents in the stator bars embedded in the slots and in the cage rotor are modelled and taken into account in the field solution. The core losses are considered during post processing by making Fourier decomposition of flux

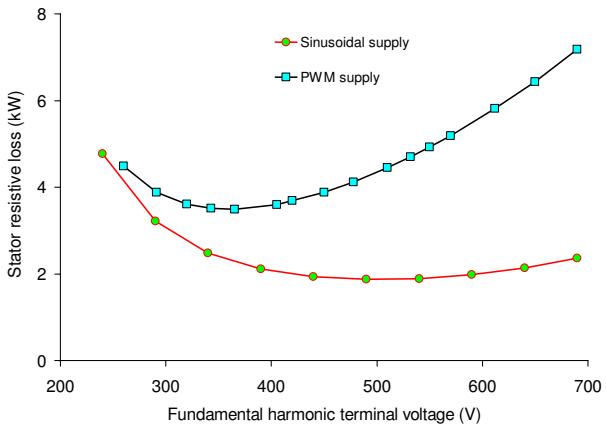

Fig. 16. The stator resistive losses are presented as a function of the FH terminal voltage at the quarter load for sinusoidal supply and PWM supply.

density. The motor is supplied from a pulse-width-modulated voltage source. A very typical case is studied when the DC-link voltage is kept fixed and fundamental harmonic voltage is decreased by increasing the flux weakening frequency. The speed has been adjusted with the voltage to achieve the particular load. For a fixed DC-link voltage, there is a very small scope to reduce the resistive losses. The total electromagnetic loss can be reduced, as the core losses always decrease with decrease the FH terminal voltage. However, if there is a possibility to use the changeable DC-link voltage, the total electromagnetic as well as the stator resistive losses can be reduced significantly at light load conditions.

Acknowledgment

The authors gratefully acknowledge the financial and technical support of ABB Oy, Finland.

References

[1] Benbouzid, M.E.H.; Beguenane, R.; Dessoude, M.; Hubbi, W.: "Energy optimizecontrol strategy for a variable input voltage three-phase induction motor", *IEEE International Electric Machines and Drives Conference Record*, 18-21 May 1997 Page(s): MD2/5.1 - MD2/5.3.

[2] Xue, X.D.; Cheng, K.W.E.: "An Energy-Saving Scheme of Variable Voltage Control for Three-Phase Induction Motor Drive Systems", *IEEE Conference Record of the 2nd International Conference on Power Electronics Systems and Applications*, 12-14 Nov. 2006, pp. 241 - 243.

[3] Lipo, T.A.: "The analysis of induction motors with voltage control by symmetrically triggered thyristors", *IEEE Transactions on Power Apparatus and Systems*, Volume PAS-90, Issue 2, March 1971, pp. 515 - 525.

[4] Mohan, N.: "Improvement in energy efficiency of Induction motors by means of voltage control", *IEEE Transactions on Power Apparatus and Systems*, volume PAS-99, Issue 4, July 1980, pp. 1466 - 1471.

[5] Jamil Asghar, M.S.; Haroon Ashfaq: "Speed control of wound rotor induction motors by AC regulator based optimum voltage control", *IEEE Conference Record of the 5th International Conference on Power Electronics and Drive Systems*, Volume 2, 17-20 Nov. 2003 pp. 1037 - 1040.

[6] Boglietti, A.; Bottauscio, O.; Chiampi, M.; Pastorelli, M.; Repetto, M: "Computation and measurement of iron losses under PWM supply conditions", *IEEE Transactions on Magnetics*, Volume: 32, Issue: 5, September 1996, pp. 4302-4304.

[7] Arkkio, A.: "Finite element analysis of cage induction motor fed by static frequency converters", *IEEE Transactions on Magnetics*, Volume 26, Issue 2, Mar 1990, pp. 551-554.

[8] Arkkio, A.: "Analysis of a 37 kW cage-induction motor" *Laboratory of Electromechanics, Helsinki University of Technology*, Report 30, Finland, 1991, 64 p.

[9] Wu, Y.; Mcmahon, R.A.; Zhan, Y.; Knight, A.M.: "Impact of PWM schemes on induction motor losses", *IEEE Conference Record 41st IAS Annual Meeting*, Volume 2, 8-12 Oct. 2006 Page(s):813 - 818.

[10] Salon, S.J.; Ovacik, L.; Balley, J.F.: "Finite element calculation of harmonic losses in AC machine windings", *IEEE Transactions on Magnetics*, Volume 29, Issue 2, March 1993, pp. 1442-1445.

[11] Hilderbrand, E.N.; Roehrdanz, H.: "Losses in three-phase induction machines fed by PWM converters", *IEEE Transactions on Magnetics*, Volume 16, Issue 3, September 2001, pp. 228-233.

[12] Lee, J.J.; Kim, Y.K.; Nam, H.; Ha, K.H.; Hong, J.P.; Hwang, D.H.: "Loss distribution of three-phase induction motor fed by pulsewidth-modulated inverter", *IEEE Transactions on Magnetics*, Volume 40, Issue 2, March 2004, pp. 762-765.

[13] Islam, M.J.; Arkkio, A: "Effects of pulse-width-modulated supply voltage on eddy currents in the form-wound stator winding of a cage induction motor", *IET Electric Power Applications*, In press.

[14] Holmes, D.G; Lipo, T.A.: "Pulse width modulation for power converters principle and practice", *IEEE Series on Power Engineering*,A John Wiley and Sons, inc., Publication 2003, 724 p.

[15] Meco-Gutirrez, M.J.; Prez-Hidalgo, F.; Vargras-Merino, F.; Heredia-Larrubia, J.R: "Pulse width modulation technique with harmonic injection and frequency modulated carrier: formulation and application to an induction motor", *IET Electric Power Applications*, volume 1, issue 5, September 2007, pp. 714-726.

[16] Islam, M.J.; Pippuri, J.; Perho, J.; Arkkio, A: "Time-harmonic finite-element analysis of eddy currents in the form-wound stator winding of a cage induction motor", *IET Electric Power Applications*, volume 1, issue 5, September 2007, pp. 839-846.

[17] Islam, M.J.; Arkkio, A: "Time-stepping finite element analysis of eddy currents in the form-wound stator winding of a cage induction motor supplied from a sinusoidal voltage source", *IET Electric Power Applications*, In press.

[18] Yatchev,I.; Arkkio, A.; Niemenmaa, A.: "Eddy-current losses in the stator winding of cage induction motors", *Laboratory of Electromechanics, Helsinki University of Technology*, Report 47, Finland 1995, p. 34.

[19] Arkkio, A.: "Analysis of induction motors based on the numerical solution of the magnetic field and circuit equations", *Acta Polytechnica Scandinavica, Electrical Engineering series No. 59*, Helsinki, Finland. (1987) 97 p. http://lib.tkk.fi/Diss/198X/isbn951226076X/

[20] Belahcen, A.; Arkkio, A: "Comprehensive dynamic loss-model of electrical steel applied to FE simulation of electrical machines", *CD proceedings of the 16th International conference on Compumag*, Aachen, Germany, 24-28 June 2007, Paper PA3-7, 4p.

[21] Grant, D. A.; Stevens, M.; Houldsworth, J. A.: "The effect of word length on the harmonic content of microprocessor-based PWM wave form generators", *IEEE Transactions on Industry Applications*, Vol. IA-21, Issue 1, January/February 1985, pp. 218-225.